Available online at www.sciencedirect.com
ScienceDirect
International Journal of Mass Spectrometry 260 (2007) 166–176
International Journal of Mass Spectrometry
www.elsevier.com/locate/ijms

Imaging of small molecules in tissue sections with a new intermediate-pressure MALDI linear ion trap mass spectrometer

Timothy J. Garrett [a], Maria C. Prieto-Conaway [b], Viatcheslav Kovtoun [b], Huy Bui [b], Nick Izgarian [b], George Stafford [b], Richard A. Yost [a,*]

[a] *University of Florida, Department of Chemistry, Gainesville, FL 32611, United States*
[b] *Thermo Electron Corporation, San Jose, CA, United States*

Received 15 June 2006; received in revised form 12 September 2006; accepted 12 September 2006
Available online 31 October 2006

Abstract

We describe a new intermediate-pressure MALDI linear ion trap mass spectrometer and its capabilities for imaging mass spectrometry. The instrument design is described and is characterized in terms of four performance issues (1) MALDI performance at intermediate pressure; (2) analysis of samples on non-conductive and conductive glass slides; (3) critical importance of tandem mass spectrometry (both MS^2 and MS^3) for identification of analyte species and imaging of isobaric species; (4) capability for repeated analysis of the same tissue section. Application of the new instrument to imaging phospholipids in rat brain sections is described in detail.

Keywords: Imaging MS; MALDI; Intermediate pressure; Linear ion trap; Phospholipids

1. Introduction

Imaging thin tissue sections by mass spectrometry provides a unique opportunity to generate chemically resolved images representing the distribution of compounds present in the tissue section. Although spatial resolution has been of considerable interest, it is this chemical aspect in which imaging MS will provide expanded opportunities to the field compared to other imaging techniques such as nuclear magnetic resonance, fluorescence microscopy, and positron emission tomography. Here, we describe a novel mass spectrometric system employing laser desorption at intermediate pressure interfaced with a linear ion trap for tandem mass analysis (MS/MS and MS^n)

Mass spectrometric microprobes with matrix-assisted laser desorption/ionization (MALDI) offer a unique opportunity to directly probe thin tissue sections for changes in the distribution of molecular species of interest. Initial microprobe designs offered the opportunity to identify changes in the distribution of a desired compound in different regions of a tissue of interest [1]. Investigating the distribution of a compound within tissue sections can help understand whether an exogenous compound administered orally, such as a small drug molecule [2–6], can be found within the body, where that compound tends to localize, and possibly how endogenous compounds are affected by the drug. The latter aspect is a new concept to the field of imaging, because using a mass spectrometer begets the opportunity to gather more complete chemical information about a tissue section, including detection and identification of unknown compounds. The mapping of endogenous compounds in tissue sections offers an incredibly specific method to identify changes in the profile of the compound in diseased versus normal states [7–9].

Imaging MS can be performed on any mass spectrometer employing a MALDI (or SIMS) [10–12] source as long as the sample plate can be rastered with respect to the laser or ion beam (or the laser/ion beam rastered with respect to the sample plate). Some researchers have also shown the ability to perform imaging MS studies with a new ionization technique,

* Corresponding author at: University of Florida, Department of Chemistry, P.O. Box 117200, Gainesville, FL 32611, United States. Tel.: +1 352 392 0557; fax: +1 352 392 4651.
E-mail address: ryost@chem.ufl.edu (R.A. Yost).

1387-3806/$ – see front matter © 2006 Elsevier B.V. All rights reserved.
doi:10.1016/j.ijms.2006.09.019

desorption electrospray ionization (DESI) [13], at atmospheric pressure, but with far less spatial resolution than MALDI or SIMS. In MALDI, the laser spot size is typically anywhere from 50–100 μm. Smaller spot sizes have been obtained using small slits or over-sampling methods [10,14]; even smaller spot sizes may be possible using novel optics including near-field optical designs [15,16]. In SIMS, the spot size can be much smaller, usually a few hundred nanometers, because of the use of an ion rather than a laser beam, which offers the ability to analyze single cells [12,17,18].

In contrast to SIMS, a requirement to perform MALDI is the application of a matrix material that absorbs the energy of the laser and gently transfers some of that energy to analytes prepared with the matrix. For analysis of standards, the matrix, present at a much higher concentration, and the analyte are deposited as solutions on the surface of a metal plate and allowed to dry for co-crystallization to occur. However, this method cannot be employed in tissue imaging MS because depositing the matrix as a droplet on to the tissue surface can cause compounds in the tissue to move, thereby disturbing their original location [4,19,20]. Therefore, to perform imaging MS, the matrix is typically sprayed onto the tissue surface as very fine droplets, creating a more uniform matrix coating without causing analyte migration [4,19].

There are several commercial mass spectrometers capable of analyzing tissue samples with tandem MS, including TOF–TOF [21], Q-TOF^3, and ion trap [22]. All of these instruments are capable of analyzing small molecules from tissue sections with structural identification. Although there are advantages and disadvantages of each instrument, a comparison of each instrument is not the focus of this article. The research presented is focused on the use of a linear ion trap instrument for the imaging of tissue sections and the specific utility of MS^n and full-scan tandem MS data in analyzing tissue sections.

2. Experimental

2.1. Instrument description

The instrument used for all studies is a linear ion trap fitted with a MALDI ion source that operates at intermediate-pressure (Finnigan LTQ with vMALDI from Thermo Electron Corporation San Jose, CA). A schematic of the instrument is shown in Fig. 1. The source consists of a N_2 laser (337 nm) directed to the source by a fiber optic cable; optics outside the vacuum chamber allow for laser spot diameters from 80 to 120 μm at an incident angle of 32°. The laser spot size for these experiments was either 100 or 120 μm. The source is designed to operate at a pressure of 0.17 Torr, well above that of a standard high vacuum MALDI source, but substantially below that of an atmospheric pressure (AP) MALDI source. The standard vMALDI software limits sampling to the normal 3 mm diameter sample wells, but tissue samples larger than this were analyzed with tissue imaging software from Thermo. The sample plate consists of two parts: a bottom piece and a top plate that can be modified to accept surfaces of various shapes. The top plate for general MALDI applications is a standard 96- or 384-well microtiter plate, with dimensions of 5 in. × 3.4 in (12.7 cm × 8.6 cm). The top plate for the tissue imaging application can hold four standard microscope slides (2.5 cm × 7.5 cm, 0.1 cm thick). Double-sided tape (Scotch 1.27 cm wide, 3 M, Minneapolis, MN) was used to affix the slides to the top plate; additionally, conductive copper tape (Stewart-McDonald Athens, OH) can be used along the edges, which provides electrical conductivity between the conductive glass slides and the top plate. The vMALDI control software automatically identifies which plate configuration is being used. The sample plate mounts on the XY stage by means of spring tension clamps, and two precision vacuum-rated stepper motors control the two-dimensional movement. These actuators position the XY stage with an accuracy of better than ±3 μm. The precision in going back to a specific location is ±1 μm without taking the plate out and approximately ±7 μm after taking the plate out of the vacuum and putting it back in.

A modified set of quadrupole rods, q00, which can accommodate the entrance of the laser beam and access for camera viewing, is added to the front of the LTQ multipole arrangement to enable use of the vMALDI source (Fig. 1). The MALDI sample plate is positioned in front of the q00 arrangement. The rest of the system is identical to the standard LTQ with ESI, a q0 quadrupole, an octopole, lenses, and the linear ion trap. The linear ion trap is a high-capacity, three-part segmented trap with radial ejection of the ions to two detectors [23]. The three main components of the vMALDI source (the control, optical,

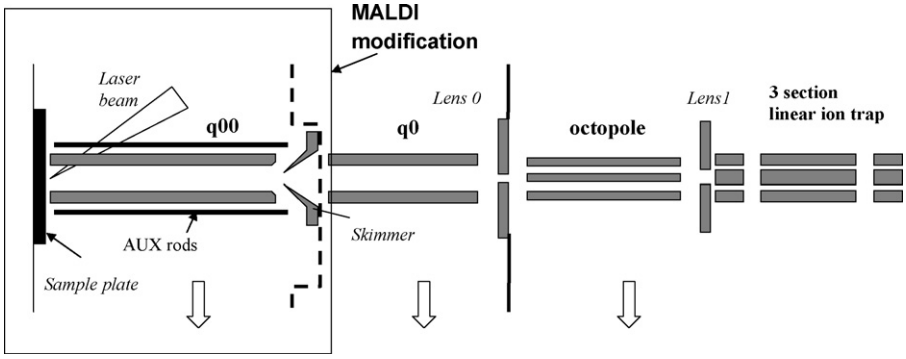

Fig. 1. Schematic of the LTQ with vMALDI source. The vMALDI source replaces the typical ESI front-end as indicated in the figure. An additional square quadrupole is added to direct ions from the sample plate into the LTQ. The laser beam is generated from a nitrogen laser (337 nm) and impinges the surface at a 32° angle measured from the ion optics axis. Mass analysis is accomplished with a three-section linear ion trap.

and sample modules) are integrated with the ion trap through firmware and electronics. Features of the LTQ, such as automatic gain control (AGC) and data-dependent MS^n methods, are thus made available to MALDI samples. AGC with the vMALDI source determines the number of laser shots to optimally fill the trap with ions, thus avoiding space charge-related peak broadening and mass shifts. Tandem mass spectrometry employing collision-induced dissociation (CID) on the LTQ can provide higher order MS^n up to $n = 10$. Three different scan rates are available to provide different degrees of mass resolution in the LTQ: normal, zoom, and ultrazoom. Unit mass resolution is available with normal scan rate through *m/z* 4000; ultrazoom scan rate provides the highest resolving power of 18,000 at *m/z* 2000.

2.2. Acquisition of position-specific mass spectra

For analyzing tissue samples, the custom software takes a picture of a desired area, 1000 μm × 1000 μm at a time. The tissue section, or other area of interest, within this picture is selected by drawing a circle, square, or free draw around the area of interest. The step size can be set to a desired value. In the case of these experiments, the step size was set to 100 or 120 μm, the same size as the laser spot size. AGC can be employed to automatically vary the number of laser shots at each point to maintain an approximately constant number of ions in the trap for each spectrum. In these studies, the same number of laser shots was used at each point across the tissue specimen by turning off AGC. The number of laser shots and the power of the laser were selected by interrogating one spot of the tissue sample. Both the power and the number of shots were adjusted in order to avoid space-charging effects that can reduce the mass resolution and mass accuracy of the instrument. Typically 10 laser shots were needed to produce a strong signal from each point on the tissue section. For initial experiments, automated MS/MS data were collected from the tissue surface on a series of ions selected by the investigator. Further MS/MS experiments were performed scanning the entire tissue for a single ion with an isolation width of 1.5. More laser shots were typically used when performing MS/MS and MS^3 experiments, usually 15–20, especially for compounds present in low abundance to ensure that enough ions were trapped to produce sufficient signal after CID. For the automated MS^2 experiments performed here, the number of laser shots was not increased because sufficient signal was present for the production of abundant MS/MS and MS^3 product ion spectra. The pattern used to scan the tissue section was a back-and-forth raster pattern from the top of the chosen area of analysis to the bottom using the desired *x* and *y* step size (100 or 120 μm). With 10 laser shots per spot and approximately 10,000 spots analyzed, a typical analysis for a brain tissue section, the total time for scanning the section was typically 2.5 h (approximately 0.9 s/spot).

2.3. Image generation—data processing

Once a tissue sample is analyzed in a position-specific manner, desired ion signals can be extracted from the data file using a custom extraction program or viewed using custom software from Thermo (vMALDI Data Browser program). The extraction program was used for the data presented here. In this process, the desired ion(s) is extracted by inputting a specific *m/z* range (usually 1.5 amu wide); the signal at each *x* and *y* value is then extracted and saved as a text file. The data can be normalized by dividing the ion signal at each *x* and *y* position by the total ion intensity at that same position using a spreadsheet program. The mass-specific image (whether MS or MS/MS) is then generated using Surfer (Golden Software, Golden, CO), a graphical program allowing for the generation of contour, surface (3D), and digital maps of the data.

2.4. Samples used for evaluation

Brain tissue from a rat (Spague–Dawley) was sectioned to a thickness of 10 μm at a temperature of −22 °C using a cryotome (Leica). The sections were placed directly onto three different types of microscope slides, plain glass, "plus" (polymer coated), and indium tin oxide (ITO) coated (conductive glass slides). The first two types of microscope slides are non-conductive and are typically used in the preparation of samples for histology; the third slide is conductive. The resistance of the ITO coated microscope slide was 40 Ω over a distance of 1 cm. The tissue was allowed to warm on the microscope slides for 10 s before refreezing and storage at −80 °C. For mass spectrometric analysis, the tissue sections were removed from the freezer and placed in a dessicator for 30 min before applying the MALDI matrix.

2.5. Matrix coating method

The matrix was applied to the tissue sections using an artistic airbrush (Aztek A470, Testors, Rockford, IL). Electrospray deposition could not be used because some of the sample surfaces used were non-conductive microscope slides. The airbrush has controls for solution and gas flow rate. The general-purpose tip (0.40 mm) was used for all matrix coatings, but the tip is easily changed from 0.30 to 1.02 mm. The solution and gas flow rates were adjusted using a blank piece of glass for evaluation of the matrix coating. These two controls allowed for the easy adjustment of droplet size and solution flow rate. After adjusting the airbrush controls, the tissue was passed underneath the spray and allowed to dry after each pass for about 30 s. A good coating slightly wetted the tissue surface with a very thin layer of matrix and solvent that evaporated rapidly, preventing the accumulation of solvent into puddles which may cause analyte migration. Slight wetting of the tissue surface is critical to allowing matrix to interact with analytes in the tissue, but excessive wetting (or puddling of solvent) could cause analytes to migrate. Excessive wetting was avoided in the procedure. An important aspect of a good coating was the deposition of enough matrix to produce a good signal from the tissue surface. The distance from the tip of the airbrush to the microscope slide was approximately 15 cm. Approximately 20 passes were required to produce a coating that provided a strong MALDI signal. The process took about 10 min for each tissue section. For most experiments, the matrix

used was 2,5-dihydroxybenzoic acid (DHB) at a concentration of 40 mg/mL in 70% HPLC grade methanol and 30% water. Sodium acetate was added to induce cationization with a final concentration of 20 mM.

3. Results and discussion

The use of increased pressure when performing MALDI has been shown to reduce the source fragmentation of labile molecules [24]. Fig. 2 shows the effect of increased source pressure of reducing fragmentation for sphingomyelin, SPM (16:0). This sample was deposited using the dried droplet method with the matrix 6-aza-2-thiothymine (ATT). SPM (16:0) was prepared to a concentration of 10 ppm in methanol. SPM is a typical lipid class present in nerve tissue samples. The top spectrum was acquired on a MALDI ion trap mass spectrometer built at UF that has a pressure of 10^{-6} Torr in the source region [25], while the bottom spectrum was acquired at an intermediate pressure of 0.17 Torr, approximately 10^5 times higher. The expected signal for SPM (16:0) would occur at *m/z* 703.6 as the $[M+H]^+$ ion and at *m/z* 725.6 as the $[M+Na]^+$ ion. Both of these ions are present in each spectrum. When operating at the lower pressure, extensive fragmentation was evident indicated by a low signal intensity for the parent ions, $[M+H]^+$ and $[M+Na]^+$. The fragment ion at *m/z* 184.1 is the dominant ion in the spectrum and is produced from in-source fragmentation either by laser-induced photodissociation or energetic collisions of the $[M+H]^+$ ion. Increasing the pressure by an approximate factor of 10^5 in the source region reduced fragmentation, doubling the signal for the $[M+H]^+$ ion. The sodiated species was also detected at 10^{-6} Torr and showed 50% fragmentation, while at higher pressure, the fragmentation was less than 10%. Each fragmentation percent was calculated by adding the intensity of the fragment and parent ions, then dividing the individual signal for each by the summed signal. The fragment ion from the sodiated species appears at *m/z* 666.8 at intermediate-pressure (bottom spectrum) and *m/z* 666.5 at 10^{-6} Torr (top spectrum). An interesting observation in the spectra at both pressures is that the protonated species exhibits a higher degree of source fragmentation than the sodiated species under the same MALDI conditions. This suggests that when analyzing phospholipids from tissue specimens, the sodiated species should be produced over the protonated species to obtain the highest signal intensity. Fortunately, tandem MS of the sodiated species also produces more abundant and more informative fragment ions, allowing for proper structural characterization [26–28]. Addition of sodium ions to the matrix before tissue coating was also used to reduce the complexity of spectra produced because the protonated species is nearly absent. However, as is described later, the addition of sodium also caused the production of multiply cationzied species, which could only be deciphered by tandem MS. The presence of excess sodium may also increase the matrix background and it may also suppress the ion signal of other species such as proteins and peptides, although an increase in the matrix background was not evident in these experiments.

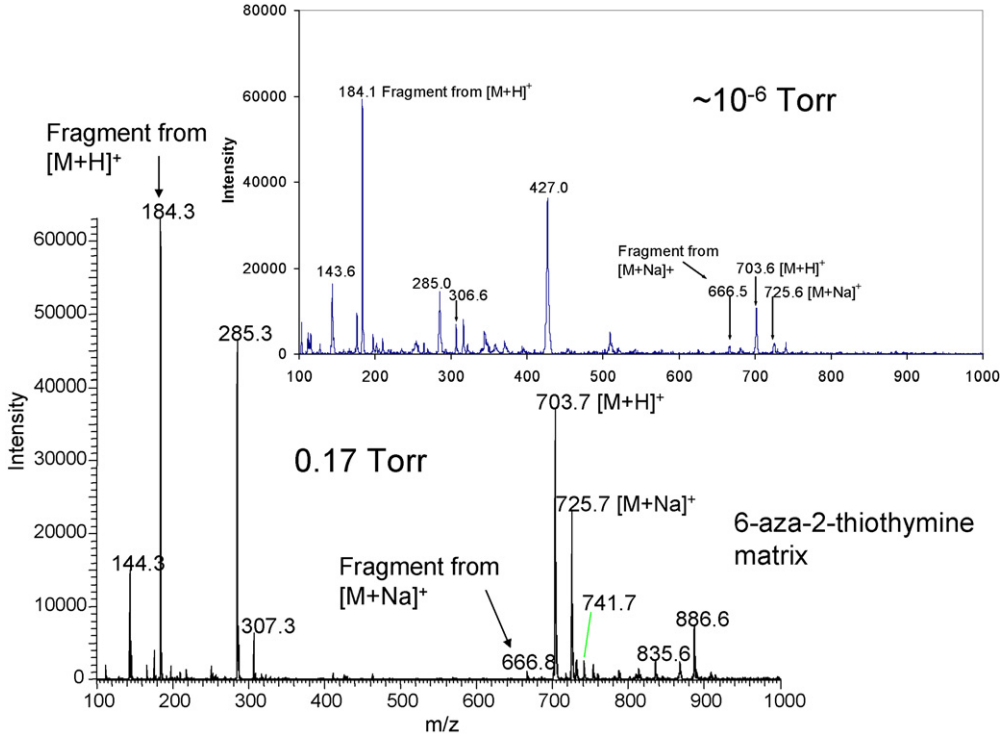

Fig. 2. MALDI spectra acquired at a pressure of ~10^{-6} Torr (Top) and 0.17 Torr (Bottom). The matrix used was 6-aza-2-thiothymine for the analysis of sphingomyelin (16:0). The traditional dried droplet method was used. By increasing the pressure in the source region, source fragmentation can be reduced, although not eliminated for the analysis of this phospholipid. Interestingly, the protonated species exhibits a greater degree of fragmentation than the sodiated species under the same conditions. The S/N ratio for the $[M+H]^+$ ion at 10^{-6} Torr is 44, while at increased pressure it is 127.

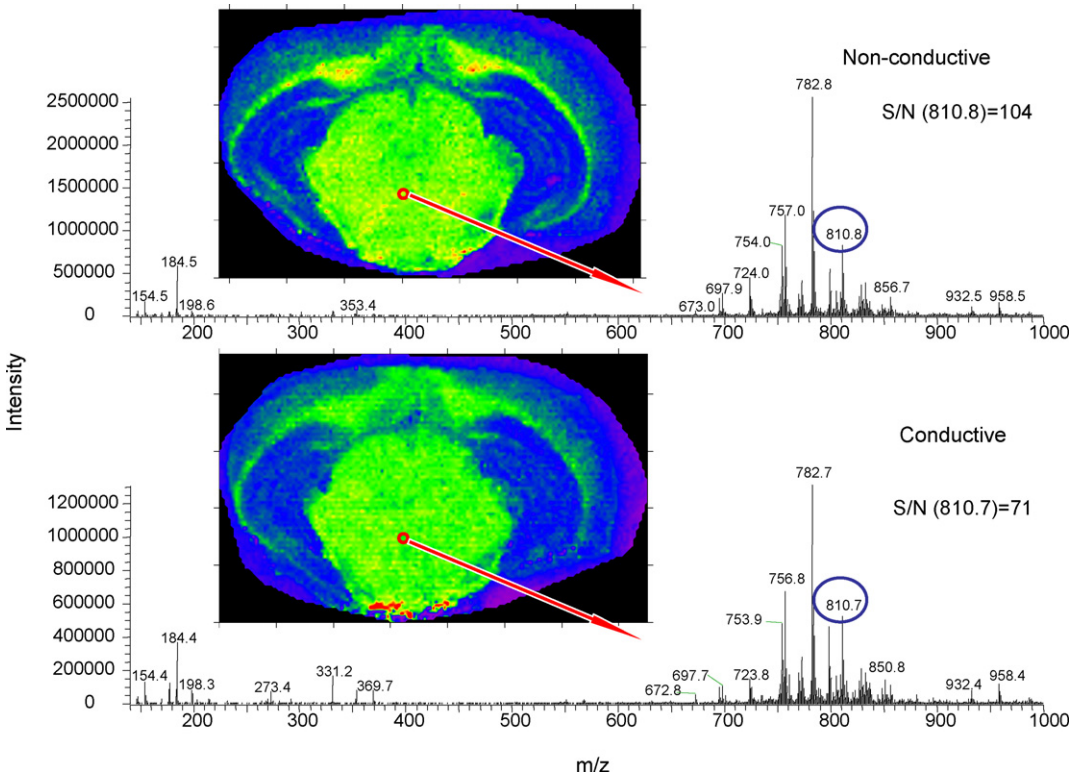

Fig. 3. Comparison of non-conductive and conductive surfaces for imaging MS. Both images in the figure are extracted for the ion at *m/z* 810. The top spectrum and image were acquired on a non-conductive glass microscope slide, while the bottom spectrum and image were acquired on a conductive glass microscope slide (indium tin oxide conductive coating). The brain tissue sections are 10 μm thick and are serial sections. Both spectra represent the same 100 μm location in the tissue (shown as a red circle in the images) and show good correlation in mass analysis.

3.1. Conductive versus non-conductive surfaces

The ability to desorb ions from glass surfaces typically used in histological techniques will allow for better combination of these traditional techniques with imaging MS. Serial brain tissue sections were placed on a non-conductive microscope slide and on a conductive microscope slide. Both samples were coated with DHB using an airbrush, and then analyzed at a step size of 100 μm with 10 laser shots per spot. Fig. 3 shows MS images for *m/z* 810, $[M+Na]^+$ phosphatidylcholine (PC) (18:0, 18:1), extracted from both the non-conductive (top) and conductive (bottom) data sets. As is seen in the figure, the images are very similar in appearance, showing the same distribution of this phospholipid in the brain tissue section. Other ions were extracted from the data set, and each ion showed a similar image on both surfaces. Single spectra collected from each sample, from the same location on the tissue, are shown in Fig. 3 as well. The spectra show similar intensities for all the major ions detected as well as equivalent *m/z* values. The same number of laser shots, 10, was collected for mass analysis at each spot across the tissue on each surface.

The use of non-conductive glass microscope slides for the imaging of tissue sections by MALDI time-of-flight mass spectrometry has been shown to decrease mass resolution and mass accuracy, especially with the addition of consecutive laser shots, because of the surface charging effect [29,30]. Surface charging is more critical in TOF analysis because of the reliance of the mass analyzer on the initial kinetic energy of the ions. Since mass analysis with the ion trap does not rely on the initial kinetic energy of the ions, changes in the kinetic energy will have little effect on the mass analysis of ions desorbed. Although only one example of tissue analysis on non-conductive substrates is shown here, routine analysis of phospholipids and small drug compounds from tissue sections placed on non-conductive microscope slides is performed regularly in our lab with the same benefits as shown here (data not shown). The use of "plus" microscope slides also showed similar performance (the production of similar MS images) to the normal glass microscope slides and the conductive microscope slides (data not shown). Future work is planned to further compare these substrates looking for trace components, such as drug compounds, as well as peptides to determine if similar performance can be obtained on both surfaces.

3.2. Tandem MS for identification

Fig. 4 shows an MS^2 spectrum for *m/z* 782 acquired from scanning the entire brain tissue section with 10 laser shots per spot. The spectrum shown is the average spectra of 10,528 spots collected across the tissue sample. This MS^2 spectrum shows one major product ion corresponding to a neutral loss (NL) of 59 (*m/z* 723.4). If this ion is a phospholipid, this neutral loss would correspond to the loss of trimethylamine from a phosphatidylcholine or a sphingomyelin ion that is cationized

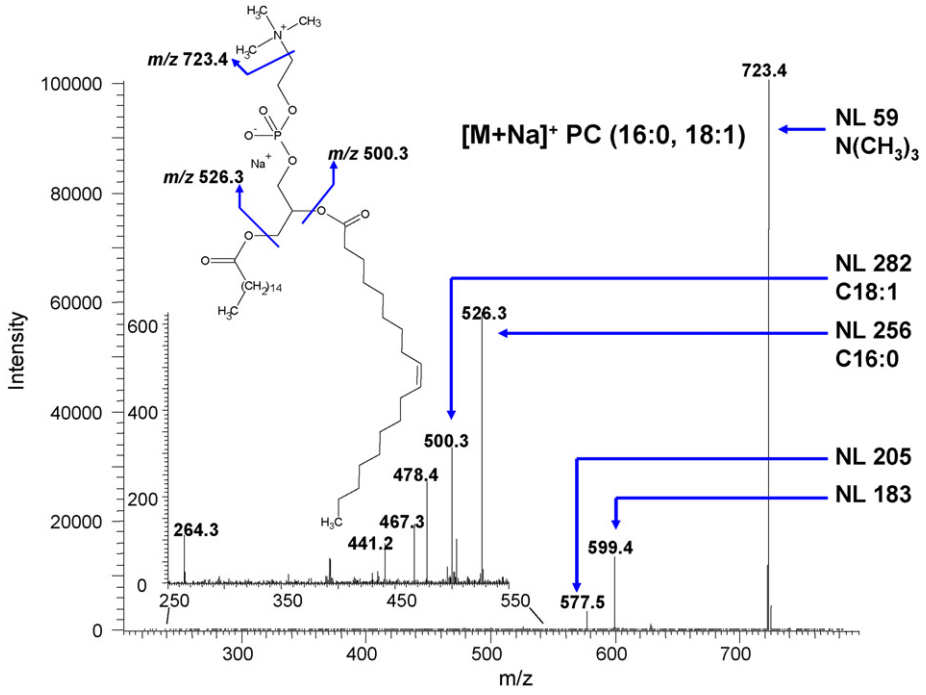

Fig. 4. Product ion spectrum (MS^2) for *m/z* 782.6. The spectrum is the average of 10,528 individual spectra acquired across the tissue surface. The mass region from 250 to 550 has been expanded to show the less abundant product ions (inset). The most abundant product ion (*m/z* 723.4) corresponds to a neutral loss of 59, trimethylamine, for a phosphatidylcholine (or sphingomyelin) ion. The ions appearing at *m/z* 526.3 and 500.3 result from losses of the fatty acid chains at *sn*-1 (526.3) and *sn*-2 (500.3) on the glycerol backbone. These allow for identification of this ion as PC (16:0, 18:1), $[M+Na]^+$.

[26–28]. If this were a protonated species, it would produce an ion at *m/z* 184 corresponding to the phosphocholine head group, as has been previously reported [22,31]. The product ions at *m/z* 599.4 and 577.5 correspond to NLs of 183 and 205, respectively. These ions represent the loss of the phosphocholine head group without sodium (*m/z* 599.4) and with sodium (*m/z* 577.5). These three product ions, along with an even parent ion mass-to-charge value, provide enough information to identify the ion as a sodiated phosphatidylcholine ion ($[M+Na]^+$) with 34 carbons and 1 degree of unsaturation in the fatty acid tails (PC 34:1) [21,22,32] The region below *m/z* 550 was expanded to show the less abundant product ions detected; fortunately, the linear ion trap provides remarkably high signal-to-noise ratios for ions of <0.1% relative abundance. Even though these ions are 80× less intense than the most abundant product ion, they are critical in the proper identification of this phosphatidylcholine ion. The product ion at *m/z* 526.3 results from the NL of palmitic acid ($[M+Na\text{-}C_{16}H_{31}O_2]^+$), while the product ions at *m/z* 500.3 and 478.4 correspond to NLs of oleic acid ($[M+Na\text{-}C_{18}H_{34}O_2]^+$) and sodium oleate ($[M+Na\text{-}C_{18}H_{33}O_2Na]^+$), respectively. Previous MS/MS studies have shown that the loss of the fatty acid at the *sn*-1 position occurs more readily than the loss of the fatty acid at the *sn*-2 position [26,31] This is represented in the product ion mass spectrum by a higher intensity for the product ion corresponding to the loss of the *sn*-1 fatty acid, *m/z* 526.3 in this example. These low abundant product ions thus allow for the proper identification of *m/z* 782 as the PC (16:0, 18:1), $[M+Na]^+$. Previous reports of tandem MS of phosphatidylcholines from tissue samples have shown an inability to fully identify the PC ions with the correct position for the fatty acid tails using the sodiated ion [21,22]. Producing the lithiated ion instead of the sodiated ion has been shown to produce more abundant product ions relating to the losses of the *sn*-1 or *sn*-2 fatty acids, but this addition may increase the complexity of the spectrum generated, since the protonated, potassiated, sodiated, and lithiated PC ions could all be generated from the tissue specimen [28,33]. Averaging 10,528 spectra provided enough reduction in the noise level to allow for the correct structural identification of this ion. The wide dynamic range of the linear ion trap [23] is critical to the successful observation of these low-abundance MS/MS product ions (300× less abundant than the most intense product ion). For less abundant PC compounds, MS^3 was performed on the product ion arising from a neutral loss of 59 to identify the position of the fatty acid tails.

3.3. Separation of isobaric ions

Although it may seem like an exhaustive experiment, scanning a tissue sample using tandem MS of a single *m/z* value may provide insight into isobaric species (ions with the same nominal *m/z*) in the tissue sample. This is critical in brain tissue because the different regions of the brain may have a varied chemical profile when analyzed by mass spectrometry. Thus, the separation of isobaric species is critical, especially when looking for endogenous compounds. A unique aspect of performing tandem MS on an ion trap is that all the product ions above the low mass cutoff are trapped and detected. If the entire tissue section is analyzed for a given *m/z* value by MS^2, then the mapping of all the product ions detected would allow for the separation of isobaric species by the image that is generated because some

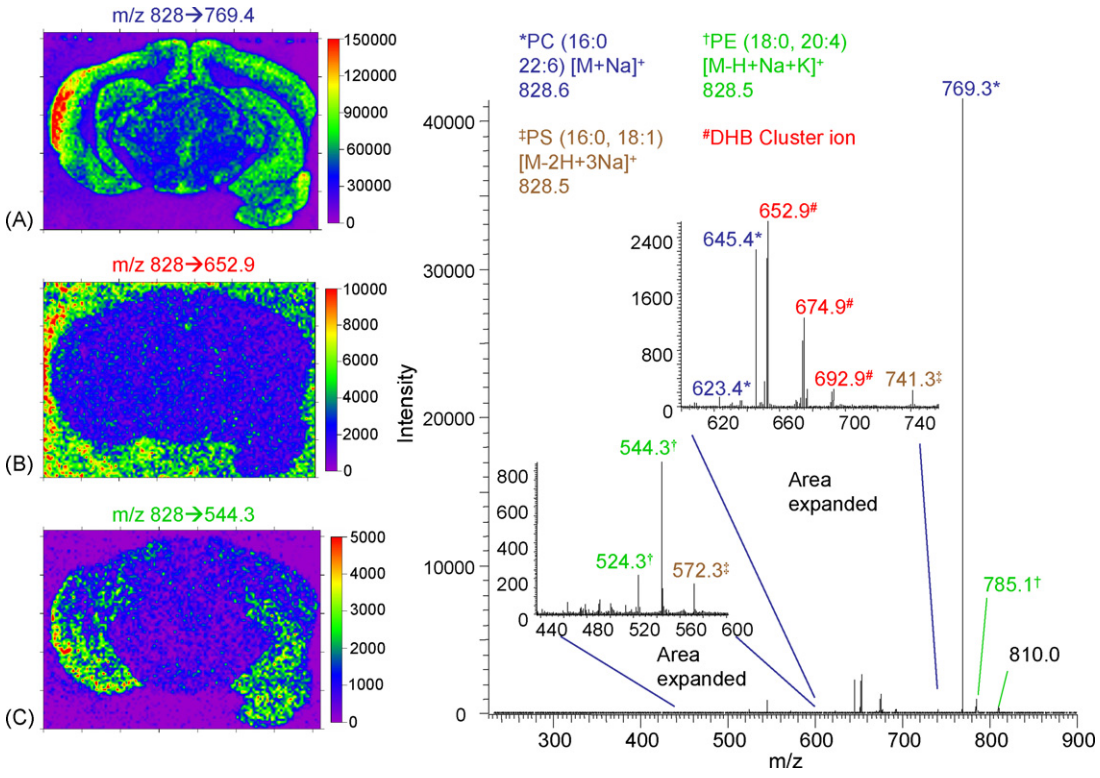

Fig. 5. Average MS^2 spectrum isolating for *m/z* 828.6 (10,528 spectra collected over the entire tissue). Specific MS images for three product ions are shown as insets. The use of MS^2 and MS^3 enabled the identification of 4 different isobaric ions appearing at *m/z* 828.6 with an isolation window of 1.5 amu. The images generated from the MS/MS product ions of the isobars (A–C) show a different distribution for each isobar. The MS/MS product ions relating to each isobar are shown with specific colors and symbols. The classification of each isobar is shown at the top of the figure. Two mass ranges are expanded and displayed as insets to show the intensity of these low-abundance product ions with respect to the overall spectrum.

isobars may have a different distribution in the tissue sample. An example of this feature is shown in Fig. 5. The spectrum in the figure is MS^2 of *m/z* 828.6 with a 1.5 wide isolation window and 30% collision energy, averaged over 10,528 spots. Two mass regions were expanded, shown as insets in Fig. 5, to show the less abundant product ions. The major species at *m/z* 828.6 was identified as PC (16:0, 22:6), $[M+Na]^+$. The product ions at *m/z* 769.4 (NL of 59), 645.4 (NL of 183), and 623.4 (NL of 205) were used to identify the phospholipid class as PC and the type of ion as $[M+Na]^+$. Since product ion spectra were collected across the entire tissue MS images (product ion images) could be generated from each product ion. The product ion image for the MS/MS product ion at *m/z* 769.4 is shown in Fig. 5A. MS^3 was performed on the product ion at *m/z* 769.4 to determine the composition of the fatty acid tails, and product ions were detected enabling the classification of the major ion at *m/z* 828 as PC (16:0, 22:6), data not shown. When product ion images were created from other product ions in the MS/MS spectrum, a single unified image was not obtained. Instead, different distributions were generated, indicating that several isobaric species were present. The most obvious isobaric species that can be identified from the spectrum is a DHB cluster ion, the matrix used for these MALDI experiments. The NLs of 176 (*m/z* 652.9), 154 (*m/z* 674.9), and 137 (*m/z* 692.9) correspond to a sodiated DHB molecule, DHB, and DHB less water, respectively. The image generated for the MS/MS product ion *m/z* 652.9 is shown in Fig. 5B. The image shows higher intensity for this ion outside the tissue section, indicating that it is not likely present in the tissue section. A MALDI matrix cluster ion is typically more intense off the tissue (when only DHB is present on the sample plate) than on the tissue, where the DHB molecules interact with many other compounds.

Two other isobaric ions were identified from this single MS/MS experiment. The product ion arising from a neutral loss of 43 at *m/z* 785.1 corresponds to the loss of aziridine from a cationized phosphatidylethanolamine, PE, $[M+Na]^+$ [34]. Additionally, it has also been shown that PE species can exchange two cations for protons, and that MS/MS of those ions shows an abundant product ion relating to the loss of the fatty acid at *sn*-1 [34]. A loss of 284 has been shown to correspond to stearic acid for PC ions, and this neutral loss is present in the MS/MS spectrum at *m/z* 544.3. However, MS/MS of a sodiated PC ion does not show a product ion that is as intense as the product ion detected in this experiment. Generating the image for this product ion (Fig. 5C) shows a different distribution in the tissue than either the DHB cluster ion (MS image 5B) or PC (16:0, 22:6) (MS image 5A). Using the ability to generate MS/MS images and performing MS^3 on selected ions, it was determined that the MS/MS product ions at *m/z* 785.1, 544.3, and 524.3 were from the same compound, namely PE (18:0, 20:4). The ionization of this compound was determined to be $[M-H+Na+K]^+$ based on previous results [34].

Finally, the fourth ion that could be identified from this data set was determined to be a phosphatidylserine, PS. This was

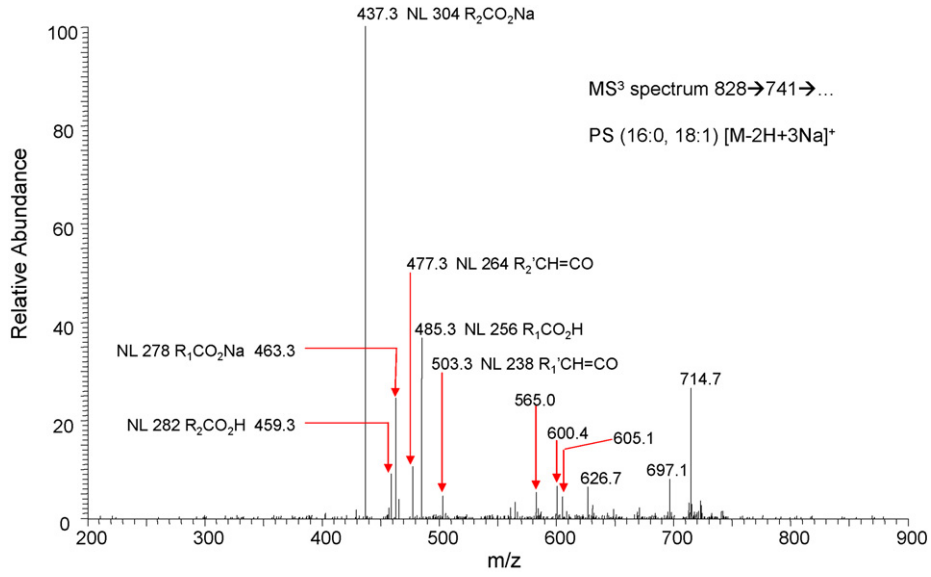

Fig. 6. The average MS^3 spectrum of 828 → 741 → . . .. The neutral loss of 87 in the MS^2 spectrum indicated that this isobar is probably a PS ion. The MS^3 spectrum shows several product ions that enable the identification of this ion as PS (16:0, 18:1), $[M-2H+3Na]^+$. A neutral loss of 256 at *m/z* 485.3 identifies palmitic acid (16:0) as the fatty acid at *sn*-1 and a neutral loss of 282 at *m/z* 459.3 identifies oleic acid (18:1) as the fatty acid at *sn*-2.

identified primarily by the presence of a product ion arising from NL of 87 at *m/z* 741.3. This is a typical loss of cationized PS ions as has been described previously [35]. PS compounds can form four major ions, primarily sodiated species, when generated by MALDI or ESI in positive ion mode, and when the appropriate counter ions are present. These ions are $[M+H]^+$, $[M+Na]^+$, $[M-H+2Na]^+$, and $[M-2H+3Na]^+$. Other ions can also be generated with variations in the cation. When subjected to CID, each of these ions show different fragmentation patterns, thus allowing for not only the identification of the species, but also the specific ion; this also results in a more complex MS/MS spectrum. When MS^3 was performed on the product ion signal at *m/z* 741.3 (arising from the neutral loss of 87 from the parent ion), a spectrum was generated that was similar to the ion $[M-2H+3Na]^+$ generated from a standard of PS (16:0, 18:1) by ESI on an ion trap [35] The MS^3 spectrum (828 → 741 →. . .), shown in Fig. 6, was generated by analyzing the entire tissue section collecting 15 laser shots per spot. The average spectrum shown in the figure represents over 10,000 spectra. The MS^3 product ion at *m/z* 485.3 is a neutral loss of 256 and results from the loss of palmitic acid, 16:0 (R_1CO_2H). Product ions at *m/z* 463.3 and 503.3 are associated with the loss of sodium palmitate (R_1CO_2Na) and palmitic acid as a ketene ($R_1CH{=}CO$), respectively. Product ions at *m/z* 477.3, 459.3, and 437.3 are associated with losses of the fatty acid at *sn*-2. These ions are identified as the loss of oleic acid as a ketene ($R_2CH{=}CO$), the loss of oleic acid (R_2CO_2H), and the loss of sodium oleate (R_2CO_2Na), respectively. The ratio of *m/z* 485.3–459.3 allows for proper assignment of palmitic acid to *sn*-1 and oleic acid to *sn*-2 [35]. The comparison to published results of standards and tandem MS enabled for proper identification of the PS ion as $[M-2H+3Na]^+$ of PS (16:0, 18:1) [35]. In total, 4 different isobaric ions were identified using MS images of product ions from MS^2 and utilizing MS^3 to further characterize PS and PE ions. It has been reported that the high abundance of phosphatidylcholine tends to prevent the detection of other phospholipid species when using MALDI in positive ion mode on a time-of-flight mass [36]. In contrast, by using tandem MS on the linear ion trap, it is possible to identify other, less abundant, phospholipids, such as PE and PS, by MALDI in positive ion mode. Furthermore, it is possible to identify these less abundant phospholipids, even when they occur at the same *m/z* as more abundant phospholipids.

3.4. Repeated analysis

Fig. 7 shows four MS images, two collected from the first full-scan analysis of the tissue section (A and B) and two collected after running 30 separate MS^2 and MS^3 experiments over a period of 1 week on the same tissue section (C and D). Both sets of MS images show a similar profile for the specified ions extracted (*m/z* 804, $[M+Na]^+$ PC (16:0, 20:4), A and C and *m/z* 828, $[M+Na]^+$ PC (16:0, 22:6), B and D). The images are very similar, but Fig. 7C and D appear to show a more resolved image, possibly related to the removal of excess matrix material. The purpose of this experiment was to check if the signal was similar to the first run; it is remarkable that images can still be generated after so many experiments on the same tissue section, without adding more matrix. In total, 37 different experiments were run on the same brain tissue section before the matrix was nearly depleted (resulting in a ∼100× decrease in ion signal). These experiments included full-scan analysis, MS^2 of various phospholipids, and MS^3 for further identification of other phospholipids present. This allowed for the full characterization of ions in the mass range of 700–900 using the same tissue specimen. All the mass spectral data for this tissue section were acquired across the entire tissue section with 10–15 laser shots per spot and 120 μm spatial resolution. The tandem MS

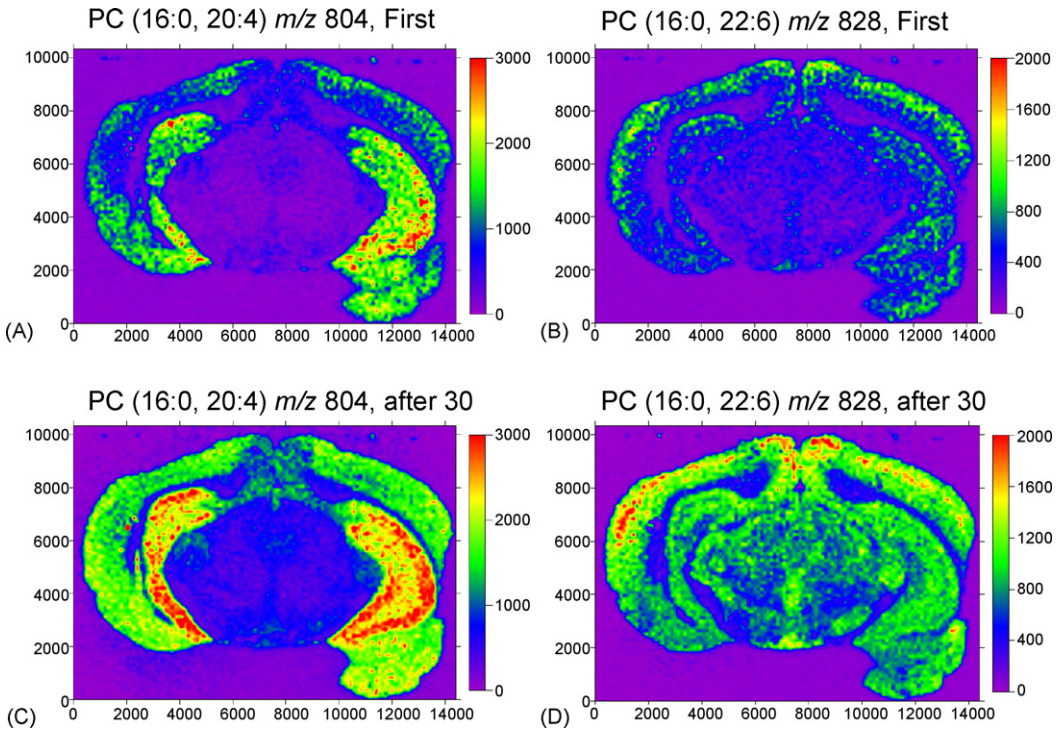

Fig. 7. MS images acquired from full-scan analysis of a brain tissue section from the first mass spectrometric data collection (A and B) and after running 30 separate experiments from the same tissue specimen before re-running the full scan (C and D). The ions shown were identified by MS^2 and MS^3 experiments (part of the 30 experiments in between the full-scan analyses). There is enough signal left in the tissue after 30 experiments (~400 laser shots at each spot) to produce a similar image of each ion, as shown.

experiments typically included more laser shots to increase the population in the ion trap and thus produce more intense fragment ions. After 37 analyses (~500 laser shots at each spot), the sample was recoated with the matrix to determine whether the signal had disappeared due to removal of matrix or removal of the analytes from the tissue section. After recoating, similar mass spectra were obtained and similar images were created with full-scan mass analysis, proving that the removal of the matrix material was the primary reason for a loss of signal. Five more MS^2 and MS^3 analyses were also performed after recoating on

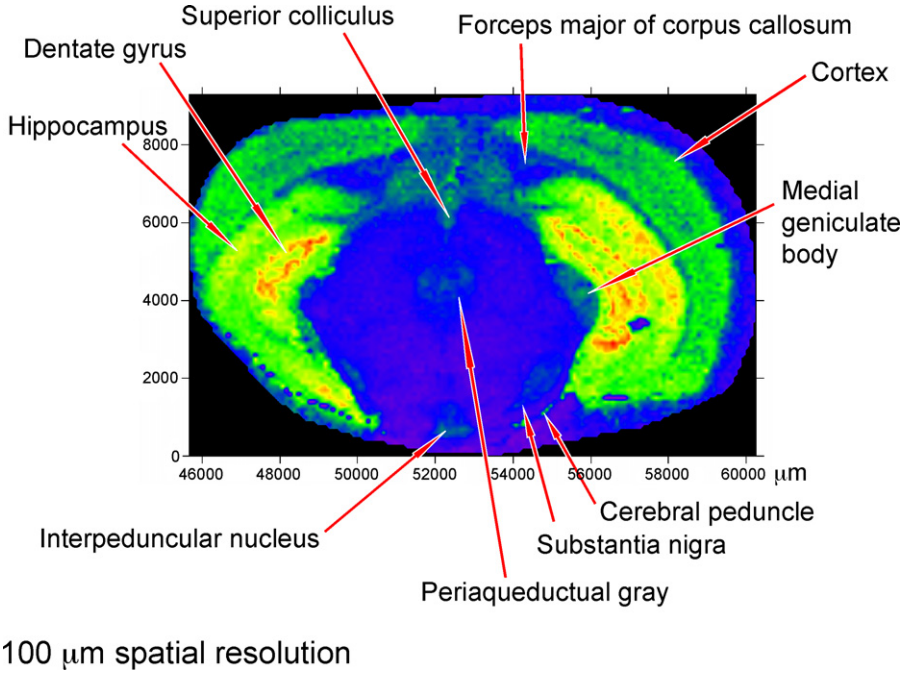

Fig. 8. MS image for *m/z* 804, PC (16:0, 20:4) showing the ability to identify substructures of the rat brain with a spatial resolution of 100 μm.

other ions from the mass spectrum. Continued analysis after recoating to determine how long the signal would last was not performed, but is of interest for future experiments as well as is the ability to re-analyze samples that are a few months old. Note that the number of successive analyses that can be performed on a tissue sample may depend on the amount of matrix and how it is applied, and perhaps the identity of the analyte and the matrix, as well as tissue sample thickness and type. Phospholipids are present in relatively high concentrations in brain tissue; therefore, the evaluation of other analyte ions such as peptides or other trace level components may require more laser shots and thus deplete the analyte and matrix signal present more rapidly, reducing the ability to reanalyze a single tissue section.

3.5. Spatial resolution

All data presented here show a spatial resolution of 100 or 120 μm (100 or 120 μm laser spot size with 100 or 120 μm step sizes). The vMALDI source provides laser spot sizes over the range of 80–120 μm. Due to the precision and accuracy of the motors employed, further reductions in the laser spot size are not limited to the mechanics of moving the sample stage and therefore would yield even better spatial resolution. Two issues that may limit the spatial resolution of the system are analyte migration due to MALDI matrix application, and reduced sensitivity when much smaller areas of the tissue are interrogated with smaller laser spots. With a spatial resolution of 100 μm, different substructures of the brain can be resolved as shown by the MS image of *m/z* 804, PC (16:0, 20:4) in Fig. 8. A rat brain atlas [37] was consulted to identify the structures of the rat brain shown in Fig. 8.

4. Conclusions

Imaging MS was successfully applied to samples analyzed by intermediate-pressure MALDI on a linear ion trap instrument. Images showed a spatial resolution of 100 or 120 μm allowing for the identification of substructures of the brain with good clarity. Better spatial resolution (around 80 μm) is obtainable, but was not evaluated on these samples. Tandem MS was successfully applied for creating MS^2 images of all product ions detected at a specified *m/z* value and MS^3 was successfully applied for further structural characterization. This enabled the identification of isobaric species in the mass spectrum. Isobaric ions were identified as phosphatidylcholines, phosphatidylethanolamines, phosphatidylserines, and DHB clusters. The large dynamic range of the instrument provided a means to structurally identify phospholipid species from brain tissue sections with using less abundant product ions from cationized species. When analyzing for species such as lipids, it is possible to run nearly 40 different experiments on the same tissue section, allowing for the positive identification of over 25 different phospholipid ions with full images generated from MS^2 data. The use of non-conductive microscope slides was evaluated, showing that comparable images could be generated, thus allowing for the use of nearly any sample surface. In conclusion, the intermediate-pressure MALDI linear ion trap instrument is a powerful new instrument for imaging mass spectrometry. Of particular importance is the utility of tandem mass spectrometry (MS/MS or MS^n) for structural characterization and for the generation of product ion images for each product ion in the mass spectrum.

Acknowledgements

Dr. Nigel Calcutt of the University of California San Diego is greatly acknowledged for providing brain tissue samples. We thank Dr. Lucia Notterpek of the McKnight Brain Institute at the University of Florida for assistance in tissue sectioning. Dr. Thomas Eskin at the University of Florida is acknowledged for his assistance in assigning brain structures. The NIH is greatly acknowledged for their support of this project (R01 ES007355).

References

[1] R. Kaufmann, R. Hillenkamp, R. Nitsche, M. Schurmann, E. Unsold, J. Micros. Biol. Cell. 22 (1975) 389.
[2] H.-Y.J. Wang, S.N. Jackson, J. McEuen, A.S. Woods, Anal. Chem. 77 (2005) 6682.
[3] M.L. Reyzer, Y. Hsieh, K. Ng, W.A. Korfmacher, R.M. Caprioli, J. Mass Spectrom. 38 (2003) 1081.
[4] F.J. Troendle, Ph.D. Dissertation, University of Florida, 2000.
[5] Y. Hsieh, R. Casale, E. Fukuda, J.W. Chen, I. Knemeyer, J. Wingate, R. Morrison, W. Korfmacher, Rapid Commun. Mass Spectrom. 20 (2006) 965.
[6] S.J. Atkinson, B. Prideaux, J. Bunch, K.E. Warburton, M.R. Clench, Chimica Oggi Chem. Today 23 (2005) 5.
[7] P. Chaurand, M.E. Sanders, R.A. Jensen, R.M. Caprioli, Am. J. Pathol. 165 (2004) 1057.
[8] P. Chaurand, S.A. Schwartz, R.M. Caprioli, J. Proteome Res. 3 (2004) 245.
[9] K. Skold, M. Svensson, A. Nilsson, X.Q. Zhang, K. Nydahl, R.M. Caprioli, P. Svenningsson, P.E. Andren, J. Proteome Res. 5 (2006) 262.
[10] R.M. Caprioli, T.B. Farmer, Gile, J. Anal. Chem. 69 (1997) 4751.
[11] M.L. Pacholski, N. Winograd, Chem. Rev. 99 (1999) 2977.
[12] N. Winograd, Appl. Surf. Sci. 203–204 (2003) 13.
[13] R.G. Cooks, Z. Ouyang, Z. Takats, J.M. Wiseman, Science 311 (2006) 1566.
[14] J.C. Jurchen, S.S. Rubakhin, J.V. Sweedler, J. Am. Soc. Mass Spectrom. 16 (2005) 1654.
[15] B. Spengler, M. Hubert, J. Am. Soc. Mass Spectrom. 13 (2002) 735.
[16] R. Stockle, P. Setz, V. Deckert, T. Lippert, A. Wokaun, R. Zenobi, Anal. Chem. 73 (2001) 1399.
[17] N. Winograd, Anal. Chem. 77 (2005) 143A.
[18] P. Sjovall, J. Lausmaa, H. Nygren, L. Carlsson, P. Malmberg, Anal. Chem. 75 (2003) 3429.
[19] S.A. Schwartz, M.L. Reyzer, R.M. Caprioli, J. Mass Spectrom. 38 (2003) 699.
[20] H.R. Aerni, D.S. Cornett, R.M. Caprioli, Anal. Chem. 78 (2006) 827.
[21] S.N. Jackson, H.-Y.J. Wang, A.S. Woods, J. Am. Soc. Mass Spectrom. 16 (2005) 2052.
[22] T.J. Garrett, R.A. Yost, Anal. Chem. 78 (2006) 2465.
[23] J.C. Schwartz, M.W. Senko, J.E.P. Syka, J. Am. Soc. Mass Spectrom. 13 (2002) 659.
[24] P.B. O'Connor, E. Mirgorodskaya, C.E. Costello, J. Am. Soc. Mass Spectrom. 13 (2002) 402.
[25] F.J. Troendle, C.D. Reddick, R.A. Yost, J. Am. Soc. Mass Spectrom. 10 (1999) 1315.
[26] X. Han, R.W. Gross, J. Am. Soc. Mass Spectrom. 6 (1995) 1201.
[27] F.-F. Hsu, J. Turk, J. Am. Soc. Mass Spectrom. 11 (2000) 437.
[28] F.-F. Hsu, A. Bohrer, J. Turk, J. Am. Soc. Mass Spectrom. 9 (1997) 516.
[29] P. Chaurand, S.A. Schwartz, D. Billheimer, B.J. Xu, A. Crecelius, R.M. Caprioli, Anal. Chem. 76 (2004) 1145.

[30] A. Scherl, C.G. Zimmermann-Ivol, J.D. Dio, A.R. Vaezzadeh, P.-A. Binz, M. Amez-Droz, R. Cochard, J.-C. Sanchez, M. Gluckmann, D.F. Hochstrasser, Rapid Commun. Mass Spectrom. 19 (2005) 605.
[31] X. Han, R.W. Gross, Proc. Natl. Acad. Sci. U.S.A. 91 (1994) 10635.
[32] S.N. Jackson, H.-Y.J. Wang, A.S. Woods, Anal. Chem. 77 (2005) 4523.
[33] Y.-P. Ho, P.-C. Huang, K.-H. Deng, Rapid Commun. Mass Spectrom. 17 (2003) 114.
[34] F.-F. Hsu, J. Turk, J. Mass Spectrom. 35 (2000) 596.
[35] F.-F. Hsu, J. Turk, J. Am. Soc. Mass Spectrom. 16 (2005) 1510.
[36] M. Petkovic, J. Schiller, M. Muller, S. Benard, S. Reichl, K. Arnold, J. Arnhold, Anal. Biochem. 289 (2001) 202.
[37] G. Paxinos, C. Watson, The Rat Brain in Stereotaxic Coordinates, fourth ed., Academic Press, San Diego, 1998.